

## Molecular Catalysts for Energy Conversion

Bearbeitet von  
Tatsuhiko Okada, Masao Kaneko

1. Auflage 2008. Buch. XXIV, 434 S. Hardcover  
ISBN 978 3 540 70730 1  
Format (B x L): 15,5 x 23,5 cm  
Gewicht: 847 g

Weitere Fachgebiete > Chemie, Biowissenschaften, Agrarwissenschaften >  
Physikalische Chemie > Katalyse, Kinetik Heterogener Reaktionen

Zu Inhaltsverzeichnis

schnell und portofrei erhältlich bei

The logo for beck-shop.de features the text 'beck-shop.de' in a bold, red, sans-serif font. Above the 'i' in 'shop' are three red dots of increasing size. Below the main text, the words 'DIE FACHBUCHHANDLUNG' are written in a smaller, red, all-caps, sans-serif font.

**beck-shop.de**  
DIE FACHBUCHHANDLUNG

Die Online-Fachbuchhandlung beck-shop.de ist spezialisiert auf Fachbücher, insbesondere Recht, Steuern und Wirtschaft. Im Sortiment finden Sie alle Medien (Bücher, Zeitschriften, CDs, eBooks, etc.) aller Verlage. Ergänzt wird das Programm durch Services wie Neuerscheinungsdienst oder Zusammenstellungen von Büchern zu Sonderpreisen. Der Shop führt mehr als 8 Millionen Produkte.

## Charge Transport in Molecular Catalysis in a Heterogeneous Phase

M. Kaneko and T. Okada

**Abstract** This chapter focuses on the fundamental aspects in controlling charge transport (CT) processes through molecules in energy conversion systems. The central reactions involved in the energy conversion are the charge separation and charge transfer processes along the reaction coordinates from reactant molecules, assisted by the catalyst active sites. In some cases the polymer medium plays an important role in the charge transport processes that are the models of molecular aggregates in biomimetic systems. The mechanism of charge transport in heterogeneous phase is discussed in detail since this makes often the rate-limiting process in the whole system, and its design is especially important to establish a high energy conversion efficiency. Charge transfer reactions at the electrode surface is outlined where the metal complex is involved as a catalyst of the redox reaction. The metal complex furnished with the functional groups and the metal active center is tailored through the optimum design of the charge transfer complexes. Finally the proton transport in a heterogeneous phase that mediates the redox and chemical reactions is introduced and its mechanism is briefly discussed.

### 2.1 Introduction

Molecule-based nano-devices are attracting a great deal of attention. They are important for catalysis especially in relevance to energy conversion, solar cells, fuel cells, and artificial photosynthetic devices that are expected to provide a renewable energy resource [1–4]. Chemical-energy-conversion devices such as fuel cells and artificial photosynthetic devices require molecular catalysts especially for multielectron redox reactions such as water oxidation, dioxygen reduction, proton reduction, hydrogen oxidation, carbon dioxide reduction, etc. [5, 6]. The development of molecular catalysts that show high activity and stability is a key research in order to create nano-devices in this field. Polymeric solid materials find promising applications as matrixes for functional molecules in these nano-devices. The development of polymeric matrixes to establish rapid charge and molecular transport is desired in relevance to molecular catalysis. In both the above materials rapid charge and

molecular transport in heterogeneous materials is required for the devices to work efficiently.

The present chapter reviews fundamental aspects in charge transport (CT) in a heterogeneous phase such as solid polymeric materials. After the introduction section (Sect. 2.1), mechanistic features of CT in polymer films and related polymeric materials confining functional redox molecules are described in Sect. 2.2, focusing especially on recent progresses in the present authors' groups. In Sect. 2.3, our attention is particularly focused on molecular CT under photoexcited state of light-absorbing molecules. CT in a fuel cell system is described in Sects. 2.4 and 2.5, where the electron transfer in the molecule is first discussed because this determines the rate of redox reactions. Typical reaction formula and elementary theory of electron transfer at the electrode–electrolyte interface under the electric field are also briefly reviewed. The dioxygen-reduction reaction is mentioned mechanistically because this is acknowledged as the major rate-limiting process in fuel cell reactions. Especially those on metal macrocycles is a matter of importance due to recent demands of noble metal-free catalysts for fuel cell developments. Finally  $\text{H}^+$  transport in a polymer electrolyte is discussed in Sect. 2.5, which is an important physicochemical process connecting  $\text{H}_2$  oxidation at the fuel electrode (the anode) and  $\text{O}_2$  reduction at the air electrode (the cathode).

## 2.2 Charge Transport (CT) by Molecules in a Heterogeneous Phase

### 2.2.1 General Overview

One of the important functions of a molecule is charge transport (CT) that is achieved mainly by redox reactions in its ground as well as photoexcited states. On incorporating molecules in a heterogeneous phase, the matrix is provided with a function of transporting charges under dark or under light irradiation, which can lead to electronic and photonic devices. In the present section, charge transport in a heterogeneous phase with incorporated redox molecules in their ground state are described, and that under photoexcited state is treated in Sect. 2.3. Both the ground and excited states electron transfer is important to obtain a complete understanding of electron transport event. So far, CT processes in ground and photoexcited states have been studied separately by the scientists in each field of electrochemistry and photochemistry, respectively. They have never been discussed together. An overview and fundamental problems on each topics will at first be given, and then the following part concentrates on the review of the results by the present authors. CT takes place by different mechanisms, i.e., physical diffusion of redox molecules, charge hopping between redox molecules, and the combined process of diffusion and charge hopping. For charge hopping the distance between the molecules which the charge can hop is especially important.

### 2.2.2 Mechanism of Charge Transport

In order to investigate charge transfer in a ground state, electrochemical technique is usually used. In this case a modified electrode coated with a heterogeneous material membrane such as a synthetic polymer containing redox molecules is utilized (Fig. 2.1). Charges are transported via redox reactions of the molecules in the matrix. This process is regarded as a kind of charge propagation. The electrochemical method provides information on integrated charge transport in the heterogeneous phase in addition to elucidating one single step of the charge transfer between molecules [4, 6, 7].

Charge propagation is understood as a diffusion of charges in a matrix, so that it is represented by an apparent diffusion coefficient ( $D_{\text{app}}$  cm<sup>2</sup> s<sup>-1</sup>). Such charge diffusion was expressed by a Dahms–Ruff equation which combines terms of physical diffusion (a kind of physical replacement) of the redox center molecules ( $D_{\text{phys}}$ ) and charge hopping between them ( $D_e$ ) (Fig. 2.2) [(2.1) and (2.2)] [8, 9], where  $k_{\text{ex}}$  is the rate constant of charge exchange between two molecules,  $\delta$  is the charge hopping distance, and  $c$  is the concentration of redox molecule in the polymer matrix.

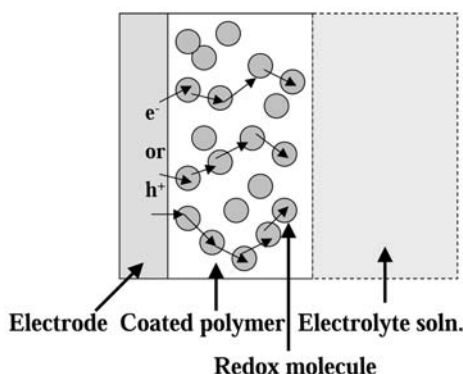
$$D_{\text{app}} = D_{\text{phys}} + D_e \quad (2.1)$$

$$D_e = k_{\text{ex}} \delta^2 c \quad (2.2)$$

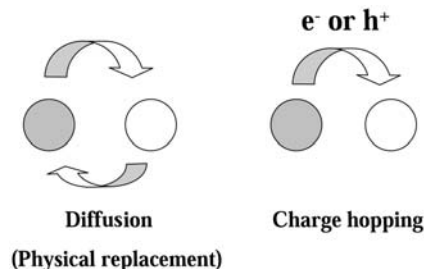
It is concluded that, if the  $D_{\text{app}}$  value is independent of the concentration, the charge transfer is contributed only by physical diffusion of the redox center, and if it is dependent on the concentration, the process is composed of both diffusion and charge hopping. Many papers reported dependence of  $D_{\text{app}}$  upon  $c$  which leads to determination of the charge transport mechanism.

Andrieux and Saveant proposed, as shown in (2.3), for a system where only charge hopping takes place [10].

$$D_{\text{app}} = (1/6)k_{\text{ex}}\delta^2 c \quad (2.3)$$



**Fig. 2.1.** Charge transport by redox molecules confined in an electrode-coated polymer membrane



**Fig. 2.2.** Charge transport mechanism by redox molecules diffusion (physical replacement) or charge hopping

It is now important that charge hopping takes place by a percolation mechanism if bounded motion of the confined charge-transporting molecules does not take place at all, where bounded motion is a kind of local oscillation of the confined redox molecules at the confined position. The charge transport by conducting carbon particles in an insulating matrix is the typical example for the percolation process although this example is not a molecular process. Such percolation process can be analyzed by a Monte Carlo simulation.

Monte Carlo simulation was carried out by Blauch and Saveant based on a percolation process, and  $D_{\text{app}}$  was obtained as (2.4) considering charge hopping and bounded motion of the redox center [11]. In this model charge transport by molecular diffusion is not taken into account.

$$D_{\text{app}} = (1/6)k_{\text{ex}}(\delta^2 + 3\lambda^2)c \quad (2.4)$$

In addition to these mechanistic studies many papers have been published by other groups.

Alternatively and more simply than the above treatments, CT mechanism by redox centers can be investigated by measuring the dependence of the initial charge transport rate ( $V_{\text{ct}}$ ) or  $D_{\text{app}}$  on the concentration of redox centers ( $c$ , represented by  $M = \text{mol dm}^{-3}$ ) in a matrix when there exists sufficient bounded motion of the redox molecules so that percolation process can be neglected. If charge propagation takes place by a diffusion mechanism (physical replacement),  $V_{\text{ct}}$  should be proportional to  $c$ . If it takes place by a charge hopping mechanism with sufficient bounded motion,  $V_{\text{ct}}$  should be proportional to  $c^2$ . However, it should be noted here that charge hopping is to be treated by a percolation theory as also mentioned later if bounded motion does not exist. These processes are represented by the following equations [12].

#### Diffusion of Redox Molecules (Physical Replacement):

$$V_{\text{ct}} = k_1 c \quad (2.5)$$

### Charge Hopping between Redox Molecules with Sufficient Bounded Motion:

$$V_{\text{ct}} = k_2 c^2 \quad (2.6)$$

### Combination of Diffusion and Hopping:

$$V_{\text{ct}} = k_1 c + k_2 c^2 \quad (2.7)$$

The mechanism can be determined by these relations or by plotting the value  $V_{\text{ct}}/c$  (or  $D_{\text{app}}$ ) against  $c$  (2.8, 2.9, and 2.10) as shown in Fig. 2.3. Instead of the  $V_{\text{ct}}$  values,  $D_{\text{app}}$  can also be used for determining the mechanism the same as the above treatment.

$$V_{\text{ct}}/c = k_1 \quad (2.8)$$

$$V_{\text{ct}}/c = k_2 c \quad (2.9)$$

$$V_{\text{ct}}/c = k_1 + k_2 c \quad (2.10)$$

Besides the charge transport rate, the fraction of the redox molecule which accepts charge(s) ( $R_{\text{ct}}$ ) is another important factor to represent the characteristics of the charge transport. In a diffusion mechanism  $R_{\text{ct}}$  is usually independent of  $c$  and reaches a high value of more than 0.8–0.9 after saturation, or sometimes it decreases when  $c$  is too high due to hindrance of molecular diffusion. The  $R_{\text{ct}}$  value after saturation of the charge propagation against  $c$  is shown in the Fig. 2.4. In a hopping mechanism  $R_{\text{ct}}$  is strongly dependent on  $c$  and with sufficient bounded motion (*vide supra*),  $R_{\text{ct}}$  can increase with the increase of  $c$ . However, without or with insufficient bounded motion,  $R_{\text{ct}}$  can increase only when  $c$  is high enough (percolation threshold) since charge hopping is possible only when a nearest neighboring molecule is located within a charge hopping distance.

When a matrix such as a polymer membrane was used to incorporate redox molecules, charging current flows giving overestimate of the charges oxidizing or reducing the redox molecules. It is therefore recommended to measure the real redox state change of the molecules by adopting in situ visible

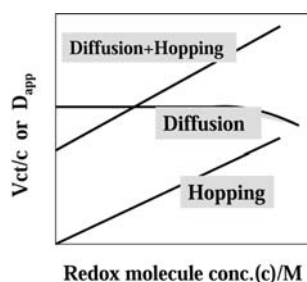


Fig. 2.3. Determination of charge transport mechanism

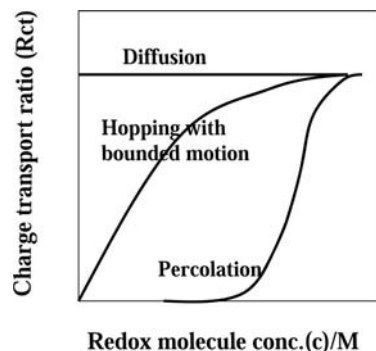


Fig. 2.4. Charge transport ratio depending on mechanism

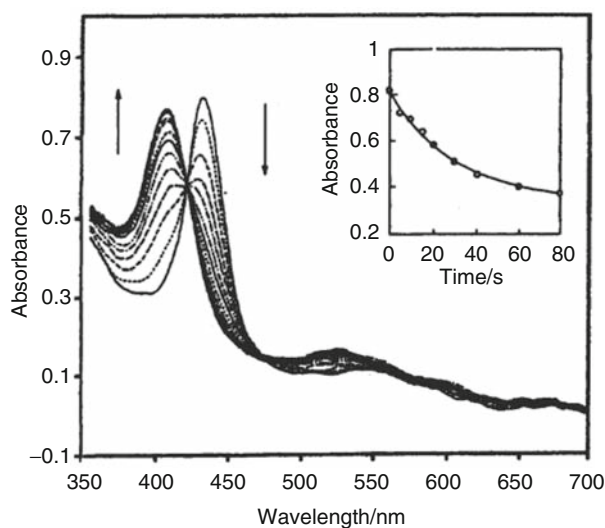
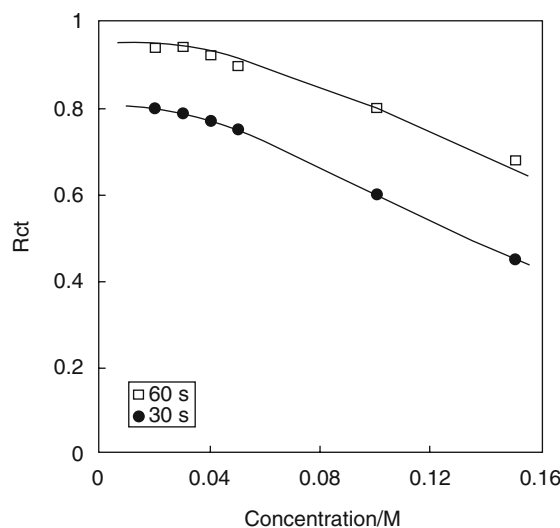


Fig. 2.5. Visible absorption spectral change of 0.1 M  $[\text{Co(III)TPP}(-2)]^+$  incorporated into a Nafion membrane soaked in a 0.1 M  $\text{NaClO}_4$  aq. soln. at pH 1.2 under potential step from 0.6 to  $-0.55$  V (vs. Ag–AgCl). Inset: decrease in absorbance at 430 nm with time ([13], copyright John Wiley & Sons, Ltd.)

absorption spectral change measurement following potential step in an electrochemical measurement; this was called spectroscopic voltammetry (SCV) or potential-step chronoamperospectrometry (PSCAS) [4,6]. One example is the CT by tetraphenylporphyrin Co(III) complex ( $[\text{Co(III)TPP}(-2)]^+$ ) confined in a Nafion membrane coated on an indium tin oxide (ITO; transparent indium tin oxide-coated glass electrode). Visible absorption spectral change on potential step from 0.6 to  $-0.55$  V (vs. Ag–AgCl) is shown in Fig. 2.5 exhibiting clear reduction of the complex with time [13]. The inset shows the absorbance decrease at 430 nm vs. reaction time.



**Fig. 2.6.** CT ratio  $R_{ct}$  vs. concentration after potential step for reduction of  $[\text{Co(III)TPP}(-2)]^+$  incorporated into a Nafion membrane exhibiting a typical diffusion CT mechanism ([13], copyright John Wiley & Sons Ltd.)

$R_{ct}$  values are plotted against  $c$  as shown in Fig. 2.6 exhibiting a typical diffusion mechanism for which  $R_{ct}$  decreases distinctly with the concentration increase due to hindrance for molecular diffusion at higher concentrations.

The typical results on charge transport mechanism depending on the kind of redox molecules and matrix are shown in Table 2.1. The redox centers used are methyl viologen ( $\text{MV}^{2+}$ ), polymer pendant  $\text{MV}^{2+}$  ( $\text{Poly-MV}^{2+}$ ), tris(2,2'-bipyridine)ruthenium(II) complex ( $\text{Ru}(\text{bpy})_3^{2+}$ ), polymer pendant  $\text{Ru}(\text{bpy})_3^{2+}$  ( $\text{Poly-Ru}(\text{bpy})_3^{2+}$ ),  $\text{Co(II)TPP}$ ,  $\text{Zn(II)TPP}$ , tetrakis(2,2'-bipyridine)- $\mu$ -oxo-diruthenium(II,III) ( $[(\text{bpy})_2\text{RuORu}(\text{bpy})_2]^{3+}$ ), and  $[(\text{NH}_3)_5\text{Ru-O-Ru}(\text{NH}_3)_4\text{-O-Ru}(\text{NH}_3)_5]^{6+}$  (Ru-red, trinuclear Ru-ammine complex). The matrix (electrode-coated polymer membrane) is mostly Nafion (Nf), a sulfonated perfluoroalkyl polyanion (**1**).

A Nafion membrane comprises hydrophilic columns composed of anionic sulfonate groups, hydrophobic columns composed of main chains, and interlayer regions between hydrophilic and hydrophobic columns. Cationic substrate can be adsorbed well from an aqueous solution, and the adsorbed material is usually located mainly in the hydrophilic columns or interlayer regions, so that a real local concentration of the adsorbed material should be calculated by adopting a localization factor ( $\alpha$ ) which shows the degree of localization. The  $\alpha$  value was estimated as 5.1 for a Nafion film cast from its alcoholic solution, and 40 for a commercially available film [12]. In many cases the thickness of a membrane was taken as  $1\text{ }\mu\text{m}$ , concentration of redox center molecules ( $c$ )  $0.01\text{--}1\text{ M}$  ( $\text{M} = \text{molar concentration, mol dm}^{-3}$ ), and the coverage of the redox molecule  $10^{-9} - 10^{-7}\text{ mol cm}^{-2}$ .



**Table 2.1.** Summary of charge transport with typical examples

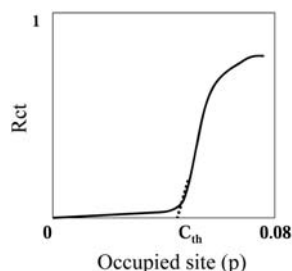
Mechanism	Rate	Bounded motion	Examples (redox center/polymer)	Dapp/cm <sup>2</sup> s <sup>-1</sup>
Physical diffusion	$V_{ct} = k_1 c$	Easy	$MV^{2+} \rightarrow MV^{+}/Nf$	11
			$Ru(bpy)_3^{3+} \rightarrow Ru(bpy)_3^{2+}/Nf$	0.85
			$[Co^{III}TPP(-2)]^{+} \rightarrow Co^{II}TPP(-2)/Nf$	4.4
			$[Co^{II}TPP(-2)]^{+} \rightarrow Co^{III}TPP(-2)/Nf$	0.73
Charge hopping	$V_{ct} = k_2 c^2$	Easy	$Ru(bpy)_3^{2+} \rightarrow Ru(bpy)_3^{3+}/Nf$	0.24
			$[Co^{III}TPP(-2)]^{+} \rightarrow [Co^{II}TPP(-1)]^{2+}/Nf$	0.03
		Difficult (but possible)	$[Zn^{II}TPP(-2)] \rightarrow [Zn^{II}TPP(-1)]^{+}/P-2VP$	0.13
			$[(bpy)_2RuORu(bpy)_2]^{3+} \rightarrow [(bpy)_2RuORu(bpy)]_2^{4+}/Nf$	
		Very difficult	$Poly-MV^{2+} \rightarrow Poly-MV^{+}$	
		Percolation	$Poly-Ru(bpy)_3^{2+} \rightarrow Poly-Pu(bpy)_3^{3+}$	
Diffusion + hopping	$V_{ct} = k_1 c + k_2 c^2$		$Ru-red \rightarrow Ru-brown(Oxidation)/Nf$	

Nf = Nafion, P-2VP = Poly(2-vinylpyridine), Poly- = Polystyrene

The results of the Table 2.1 lead to important general behavior concerning CT mechanism as follows.

1. **Charge transport mechanism:** The mechanism is determined by the interaction of the matrix with the redox species after accepting charges. When this interaction is weak and the product can diffuse in the matrix, charge is transported by a diffusion mechanism, but when the interaction is strong and the product cannot diffuse, charge is transported by a hopping mechanism. The mechanism can therefore be different for transport of either positive or negative charges even for a same redox center/matrix system. Typical example for this is the  $\text{Ru}(\text{bpy})_3^{2+}$ /Nafion system.
2.  $R_{\text{ct}}$  (fraction of redox molecule-accepting charges): For a diffusion mechanism,  $R_{\text{ct}}$  value after saturation of charge transport is independent on the redox center concentration ( $c$ ), and usually high reaching 0.8–1. For a hopping mechanism,  $R_{\text{ct}}$  is strongly dependent on  $c$  and can increase only at high concentrations.
3.  $D_{\text{app}}$ : For a diffusion mechanism apparent diffusion coefficient of the charge ( $D_{\text{app}}$ ) is independent of  $c$ , or often decreases with  $c$ , and usually shows a relatively high value of the order of  $10^{-8}$ – $10^{-10} \text{ cm}^2 \text{ s}^{-1}$ . For a hopping mechanism  $D_{\text{app}}$  is dependent on  $c$ , usually shows a low value of the order of less than  $10^{-11} \text{ cm}^2 \text{ s}^{-1}$ , and can increase only at high concentrations.
4. **Diffusion of large molecules:** Large and hydrophobic molecules such as metal tetraphenylporphyrins and metal phthalocyanines incorporated by a mixture casting method are located mainly in the hydrophilic columns or interlayer regions of Nafion, and can diffuse there exhibiting fairly high  $D_{\text{app}}$ .
5. **Redox molecules covalently attached to polymers:** CT takes place only by a hopping mechanism even when the corresponding monomeric molecule transports charges by a diffusion mechanism.
6. **Percolation mechanism:** When it is difficult for both diffusion and bounded motion to occur, the charges are transported by a percolation process. According to the percolation theory, probability of charge propagation (percolation) ( $P$ ) against redox center concentration is expressed by a sigmoidal curve.  $R_{\text{ct}}$  was calculated for a static percolation process by a Monte Carlo simulation. When the concentration (represented by occupied probability  $p$  of redox center) is low, charge propagation does not take place because the distance between molecules is too large for the charge to hop (Fig. 2.7). When the concentration increases, the charge starts to propagate, and  $R_{\text{ct}}$  increases steeply at a threshold concentration  $c_{\text{th}}$ .

No example is yet found for which charge is transported at first by diffusion of redox molecules and then by charge hopping between them.



**Fig. 2.7.**  $R_{ct}$  vs. redox molecule concentration (represented by occupied site  $p$  in the simulation) in a percolation process

## 2.3 Charge Transfer by Molecules Under Photoexcited State in a Heterogeneous Phase

### 2.3.1 Overview

Electron transport between molecules is the most essential process in biological systems. Electron transfer in biological substances such as enzymes is very rapid, so that it is in many cases investigated by utilizing electron transfer in a photoexcited state with a laser flash photolysis technique. By this method one single reaction of an electron transfer from a molecule to another or from a functional group to another can be measured. For this purpose a specific position of an enzyme is modified with a redox center molecule such as metal complex, and electron transfer is studied with a laser flash photolysis.

In earlier times, the central metal ion of the iron heme in *cytochrome c* or myoglobin was substituted by Zn, Ru ion was coordinated to a surface imidazole of a histidine residue, and then the electron transfer from the photoexcited Zn porphyrin to the Ru moiety was investigated [14,15]. The relation between the rate constant for the electron transfer  $k_{et}$  and the spatial distance between the redox centers ( $R$ ) was represented by the known (2.11) showing that the electron transfer takes place via a spatially nearest pathway.

$$-\ln k_{et} = R \quad (2.11)$$

According to the Marcus theory [16] the rate of nonadiabatic electron transfer with weak exergonicity shows a bell-shape behavior with respect to the free energy difference ( $-\Delta G$ ) between electron donor and acceptor giving a maximum rate when  $\Delta G$  equals reorganization energy of the medium. Extensive studies have been published especially on intramolecular electron transfer in this regard. However, it is not the aim of the present section to review these works. Intermolecular electron transfer between a photoexcited redox molecule and a ground state one in a heterogeneous phase will be discussed in this section.

Electron (or charge) transfer reaction of a photoexcited molecule is investigated by the following methods:

1. Measurement of a steady state ultraviolet and visible (UV-Vis.) absorption spectrum when the back electron transfer is slow, and when the equilibrium under irradiation shifts to the product side. Such reaction is called a photoredox system. There have been not many examples of this type. When the back electron transfer is rapid, the presence of some sacrificial donor or acceptor is effective to shift the reaction to the product side and therefore to monitor the reaction.
2. Monitoring a transient absorption spectrum with a laser flash photolysis method especially when the rates of electron transfer and the back reaction (recombination) are rapid.
3. Measurement of emission intensity or emission decay (lifetime) when the photoexcited state emits light (luminescence, either fluorescence or phosphorescence), and the emission is quenched by electron transfer.

### 2.3.2 Mechanism of Charge Transfer at Photoexcited State in a Heterogeneous Phase

Emission intensity and decay of a photoexcited probe gives important information on the mechanism of the electron transfer, mobility of the probe, and nature of the microenvironment around the probe. Since electron transfer from or to an excited state of a probe quenches the emission, quenching reflects the electron transfer. The mechanism of electron-transfer quenching can in general be divided into two extreme cases (Fig. 2.8).

One is a dynamic quenching for which donor and acceptor molecules diffuse freely, collide, and react. The other is a static quenching for which the molecules do not diffuse, and when a quencher ( $Q$ ) molecule exists in a quenching sphere around the probe, it quenches the emission (electron transfer takes place).

Such quenching is analyzed by plotting relative emission intensity ( $I_0/I$ , where  $I_0$  is the emission intensity without  $Q$ , and  $I$  is that with  $Q$ ) against  $Q$  concentration according to the Stern-Volmer equation (2.12)[17, 18] (called

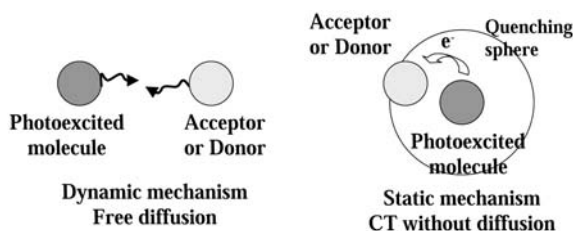
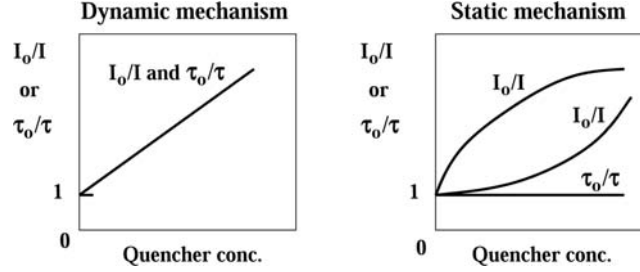


Fig. 2.8. Electron-transfer mechanism in a photoexcited state



**Fig. 2.9.** Stern-Volmer plots for typical dynamic and static-electron-transfer mechanisms

Stern-Volmer plots [17]), where  $[Q]$  is the  $Q$  concentration and  $k_{sv}$  is the Stern-Volmer constant.

$$I_0/I = 1 + k_{sv}[Q] \quad (2.12)$$

The Stern-Volmer plots based on the lifetime of the excited state ( $\tau$ , reciprocal of the first-order decay constant of the excited state) is also an important parameter to determine the electron-transfer mechanism. For a complete dynamic quenching case, both the  $I_0/I$  and  $\tau_0/\tau$  plots are linear and fall on a same line (Fig. 2.9).

For a complete static quenching case, the  $I_0/I$  plots are upwardly curved according to the Perrin equation [19] represented by (2.13) under higher concentration conditions as shown in Fig. 2.9. For this static quenching the plots  $\tau_0/\tau$  do not have a slope, i.e., the excited state involving quencher(s) in its quenching sphere does not emit at all, but the excited state involving no quencher in its quenching sphere emits the same as the system without quencher.

$$I_0/I = \exp(K_1[Q]) \quad (2.13)$$

Since  $K_1 = VN_A$  ( $V$  is the quenching sphere volume and  $N_A$  is Avogadro's number), quenching distance can be determined from the slope of  $\ln(I_0/I)$  versus  $[Q]$  plots for a static quenching case. In other static quenching cases the  $I_0/I$  plots are downwardly curved (see Fig. 2.9).

For a heterogeneous phase there exist two major problems as follows:

1. The microenvironment of the excited state is not homogeneous but different, depending on the location of the probe, which affects emission decay and quenching of the excited state. This is reflected in a multi-exponential decay of the excited state.
2. The (electron transfer) quenching mechanism can consist of both dynamic and static ones, which makes the  $I_0/I$  plots complicated. The equations to analyze electron-transfer quenching were derived based on the following standpoints [20, 21].
  - (a) The number of different sites; 1-site or 2-sites.
  - (b) Dynamic or static quenching as well as their combination.

- (c) The incorporation equilibrium of  $Q$  into the quenching sphere around a probe; one-step equilibrium or multistep one.
- (d) The rate of static quenching; either very fast so that emission is negligible, or the emission should be considered since it is competitive with the quenching.
- (e) For multistep equilibria between  $Q$  and probe; the static quenching rate is proportional to the number of  $Q$  in the quenching sphere, or independent of the number of  $Q$ .

Based on these factors 11 models and corresponding equations have been proposed for 1-site model, and 2 models for 2-site model as reported [20].

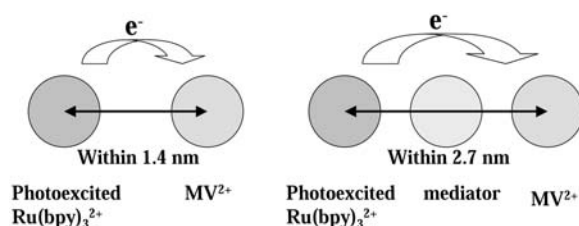
For a complete static quenching case (2.14) was derived considering the size of the probe by assuming that the probes are distributed randomly in a matrix [20],

$$I/I_0 = \exp [-4\pi (R_0^3 - s^3) N_A 10^{-24} [Q]/3] \quad (2.14)$$

where  $R_0$  is the electron-transfer distance (nm, center-to-center of donor and acceptor),  $s$  is the contact distance between donor and acceptor (nm),  $[Q]$  is the  $Q$  concentration ( $\text{mol dm}^{-3}$ ) in the matrix.

In a polysiloxane film containing dispersed  $\text{Ru}(\text{bpy})_3^{2+}$  and  $\text{MV}^{2+}$ , electron-transfer quenching of the photoexcited Ru complex by  $\text{MV}^{2+}$  was investigated [21]. The Stern-Volmer plots for the relative emission quantum yield (equals to  $I_0/I$ ) and relative lifetime of the excited state ( $\tau_0/\tau$ ) were plotted against  $\text{MV}^{2+}$  concentration. A flat (no slope)  $\tau_0/\tau$  plots showed evidently that the electron-transfer quenching takes place by a static mechanism. By applying the (2.14) ( $s = 0.82 \text{ nm}$ ), the electron-transfer distance  $R_0$  was obtained as  $1.4 \text{ nm}$  (Fig. 2.10) that is a similar value as the ground state electron-transfer distance obtained by an electrochemical method, and is also a reasonable value considering the electron-transfer distance in biological systems often reported to be around  $1.3 \text{ nm}$ .

In biological systems proteins mediate electron transfer. This mediation takes place either through bonds of the protein, or through space for which aromatic amino acid residues are considered to mediate the electron transfer in the space. Aromatic amino acid residue model, 3-methylindole as a model of



**Fig. 2.10.** Static electron transfer from photoexcited  $\text{Ru}(\text{bpy})_3^{2+}$  to  $\text{MV}^{2+}$  in a polysiloxane film in the absence and the presence of mediator (3-methylindole), a tryptophan model

tryptophan residue, was codispersed in the above  $\text{Ru}(\text{bpy})_3^{2+}/\text{MV}^{2+}$  system. In the presence of the mediator model the electron transfer was enhanced very much [20]. An equation taking into account mediated electron transfer was derived, and applied to the results giving mediated electron-transfer distance of 2.7 nm, about twice as that without the mediator. Tryptophan itself or a model of tyrosine (*p*-Cresol) was not effective for the mediation.

Electron-transfer quenching of excited  $\text{Ru}(\text{bpy})_3^{2+}$  by  $\text{MV}^{2+}$  incorporated in a poly(ethylene oxide) film took place both by static and dynamic mechanisms different from the above polysiloxane film, and the electron-transfer distance was 1.7 nm [22].

These and other results showed that electron transfer in a heterogeneous phase takes place usually by a static mechanism, but a dynamic mechanism can also be involved when diffusion or bounded motion of the redox molecules in the polymer matrix is possible. Electron-transfer distance in a photoexcited state studied by a photochemical method is in principle comparable to that in a ground state investigated by electrochemical methods.

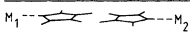
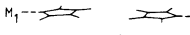
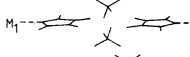
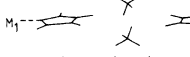
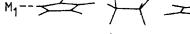
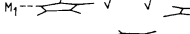

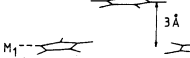
## 2.4 Charge Transfer and Electrochemical Reactions in Metal Complexes

### 2.4.1 Charge Transfer in Metal Complexes

Redox reactions occurring between two metal complexes (or a complex and an electrode) can be categorized into two mechanisms in view of the configuration of ligands surrounding the central metal ions [23]. One is outer-sphere reaction and the other is inner-sphere reaction. Outer sphere reaction is defined as the case where electron transfer occurs in the metal complex, without exchange reactions of ligands, or at least no chemical bonds are broken or formed between the metal and ligands. On the other hand, in the inner-sphere reaction, reacting metal complexes transfer ligand(s) or go through an activation state connected with bridged ligands between two complexes (or a complex and an electrode). In the latter mechanism breaking and forming of bonds between ligands and metal centers of reacting complexes occur in combination with the electron transfer.

Whether the outer-sphere reaction or the inner-sphere reaction occurs is determined by relative speed of the molecular arrangement of ligands and that of electron transfer. The outer-sphere mechanism would occur preferentially when (1) the redox reaction rate is much faster than the ligand exchange reaction, and (2) the bonding distance between the metal center and the ligand does not change much with the valence change of the central metal. If the ligand-metal structure needs to change by strong interactions and causes a high energy of rearrangement, the possibility of charge transfer becomes small. Marcus theory incorporates the reorganization energy as a principal contribution to the transition state of reacting species in the rate equations

**Table 2.2.** Calculated values of  $|\Delta|$  for bridges consisting of pyrrole ligands of  $M_1$  and  $M_2$  ( $=Fe$ ) and different inserted molecules ([26], copyright Royal Society of Chemistry)

	inserted molecule	Fe...Fe distance/Å	$\Delta/10^3$ a.u.
	—	11.2	1.6
	—	13.2	0.014
	$2 \times CH_3$	13.2	3.4
	$2 \times CH_3$	15.2	0.14
	$C_2H_5$	15.2	0.72
	$2 \times H_2O$	15.2	0.014
	$C_6H_6$	15.2	1.26
	$C_6H_6$	15.2	0.023

[16, 24, 25]. The electron transfer at the electrode with the complex or redox reactants is discussed in Sect. 2.4.2.

The electron conduction inside molecules becomes a central problem when one considers electron transfer between separate redox sites. S. Larsson studied the electron transfer between metal centers in proteins and concluded that connecting bridges (saturated or aromatic rings) with orbital energies close to the metal orbitals give rise to high transfer capabilities, the transfer range extending more than 1.5 nm [26]. Also conjugated double bonds or  $\pi$ -bonds in the moiety facilitate non-localized electron transfer as compared with  $\sigma$ -transfer in the same bridges. The probability for electron transfer is proportional to the square of energy gap parameter  $\Delta$ , which is expressed as a function of the transfer capability between adjacent atomic orbitals of the bridge compounds. Table 2.2 presents the calculated value of  $\Delta$ , for which electron transfer becomes probable for  $\Delta > 10^3$  a.u. A conjugated  $\pi$  system transfer electrons well, but saturated aliphatic or peptide chain also serves in so far as they fill the gap between the ligands [26]. The rate of long-range ( $>0.5$  nm) electron transfer, in organic and metal complexes, proteins, and intermolecular electron transfer, falls off exponentially with distance  $R$  [27].

$$k_{ET} = k_0 \exp[-\beta(R - R_0)] \quad (2.15)$$

It is noted that the charge transfer complexes are mostly furnished with conjugated systems like aromatic rings, pyrrole rings, pyridyl rings, or other heterocyclic ring chelates surrounding the metal center with specific d-band energy levels modified by the chelates [28]. N4 ligand structures around the active metal centers are characteristic features of porphyrins and phthalocyanines, which are the basic components in biological systems such as hemes of



oxygen transport or cytochromes of respiratory chains [29]. The central metal ion can be considered as the reaction site that accepts electrons from the peripheral N-containing ligand moieties. It is discussed in Sect. 1.2 (Chap. 1) that N4 ligands connect the electronic levels of the reactants and the central metal if those are too far apart, and ease the transition of electrons.

The reaction formulas often show a common feature if the reaction proceeds through single rate-determining step. In an enzymatic reaction, the substrate that reacts with the enzyme often interacts with the central metal, forms a complex, and then this complex turns into a product regenerating the original enzyme [29]. The enzyme works as a catalyst.



Here  $S$  is substrate,  $SE$  is the substrate–enzyme complex and  $P$  is product. With increasing the substrate concentration  $[S]$ , the reaction rate  $v$  levels off and approaches a saturated value  $V$  because the process is rate-limited by the amount of  $SE$ . Michaelis–Menten formula gives [29]

$$v = V \frac{[S]}{[S] + K_m} \quad (2.17a)$$

where  $K_m$  is Michaelis constant:

$$K_m = \frac{[S][E]}{[SE]} = \frac{k_{-1} + k_{+2}}{k_{+1}} \quad (2.17b)$$

with  $k_{+1}$ ,  $k_{-1}$  and  $k_{+2}$  being forward and reverse rate constants of reaction (2.16a), respectively, and that of reaction (2.16b).

Suppose that the catalyst  $E$  is adsorbed on the surface of a support. The substrate  $S$  comes from the atmosphere (or liquid phase), and forms a complex in the same ways as the enzymatic reaction. Assuming the Langmuir-type adsorption of  $E$  on the surface, the reaction rate is described by the following equation,

$$v = k[S] \frac{K[E]}{1 + K[E]} \quad (2.18a)$$

$$K = \frac{\theta_E}{(1 - \theta_E)[E]} = \exp\left(\frac{-\Delta G_E^0}{RT}\right) \quad (2.18b)$$

which is similar to (2.17a), but here the surface population of  $E$  determines the rate.  $K$  is the adsorption equilibrium constant,  $\theta_E$  the coverage of  $E$ ,  $\Delta G_E^0$  the standard free energy of adsorption and  $k$  is the net rate constant.

When the electron transfer between the substrate and the electrode is involved in the reaction, the net rate is determined by the exponential function of the electric potential. Butler–Volmer equation gives the rate of charge transfer at the electrode surface as a function of the electrode potential [30]:

$$v = k_{\text{ox}}[R] \exp\left(\frac{\alpha F(E - E_0)}{RT}\right) - k_{\text{red}}[O] \exp\left(-\frac{(1 - \alpha)F(E - E_0)}{RT}\right) \quad (2.19)$$

where  $k_{\text{ox}}$  and  $k_{\text{red}}$  are the rate constants,  $[R]$  and  $[O]$  are the concentrations of species in reduced and oxidized forms, respectively,  $E$  and  $E_0$  are the electrode potential and its equilibrium value and  $F$ ,  $R$ , and  $T$  have usual meanings. If the preceding reaction involves adsorbed intermediates, combination of (2.18a) and (2.19) makes the rate equations complex, but the analysis of rate equations gives a clue to the reaction route and mechanism (see Sect. 2.4.3).

### 2.4.2 Charge Transfer at Electrode Surfaces

Electron transfer between a metal electrode and reactant species is one of the most fundamental processes in electro-catalyst reactions.



Theoretical foundations were made by Gurney [31], Randles [32], Marcus [16,24], and by Gerischer [33] for the adiabatic electrode processes. Later Dogonadze and Levich developed the quantum-mechanical theory of both adiabatic and nonadiabatic electron transfer reactions [34]. In adiabatic processes, the nuclear motion of the atoms is supposed to be independent of the motion of electrons because of the large mass differences (Born-Oppenheimer approximation). Then the electronic energies (wave functions) are described as a function of nuclear configuration at each time an electronic transition occurs without the change of nuclear conformation (Frank-Condon principle). This means that the electron transfer occurs at iso-energetic levels between donor and acceptor atoms [25,35].

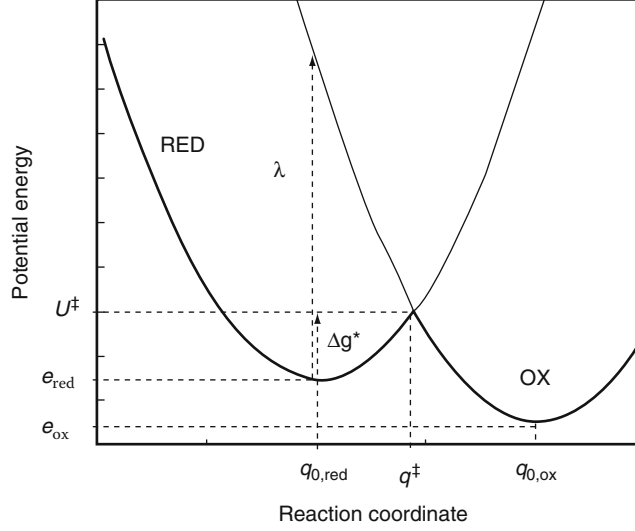
The probability  $P$  of radiationless electron transfer between reacting species and the electrode metal is given by the integral of neutralization frequency over electronic energy  $\varepsilon$ , applying the Frank-Condon principle (the nuclear configuration of species is fixed during the electron transfer) [36]:

$$P = \frac{kT}{h} \int_{-\infty}^{\infty} v(\varepsilon) N(\varepsilon) \tau(\varepsilon) \kappa(\varepsilon) f(\varepsilon) \rho(\varepsilon) d\varepsilon \quad (2.21)$$

where  $v(\varepsilon)$  is frequency factor,  $N(\varepsilon)$  the population of reactants having energies in the range  $\varepsilon$  and  $\varepsilon + d\varepsilon$ ,  $\tau(\varepsilon)$  nuclear transmission coefficient,  $\kappa(\varepsilon)$  electronic transmission coefficient,  $\rho(\varepsilon)$  the electronic density in the metal, and  $f(\varepsilon)$  the Fermi-Dirac distribution term, with the Fermi energy  $\varepsilon_F$  corresponding to half-filled electron energy [25].

$$f(\varepsilon) = \frac{1}{1 + \exp \{(\varepsilon - \varepsilon_F)/kT\}} \quad (2.22)$$

In the transition state theory, the electron transfer occurs at the point where two parabolic curves of reactants and products meet on the frame of Gibbs free energy surface along reaction coordinates (Fig. 2.11). Based on both energy conservation and the Frank-Condon principle through the potential



**Fig. 2.11.** Potential energy surface along reaction coordinates for the reaction (2.20)

energy curves in the reaction coordinate  $q$ , the rate constant for the forward (anodic) reaction is given by a transition at the intersect of two curves:

$$k_f = \nu \exp\left(-\frac{\Delta g^*}{kT}\right) \quad (2.23)$$

where  $\nu$  is the vibrational frequency along  $q$ , and  $\Delta g^*$  is the Gibbs energy difference between the transition state and the reactant system. R. A. Marcus derived a formula for redox electrode reactions using classical electrostatic models [23, 25]. The potential energy surface is approximated by the harmonic oscillator model:

$$U_{\text{red}} = e_{\text{red}} + \frac{1}{2}m\omega^2 (q - q_{0,\text{red}})^2 \quad (2.24a)$$

$$U_{\text{ox}} = e_{\text{ox}} + \frac{1}{2}m\omega^2 (q - q_{0,\text{ox}})^2 \quad (2.24b)$$

At the intercept of two curves, the coordinate gives  $q = q^\ddagger$  and  $U = U^\ddagger$ , and

$$U^\ddagger = e_{\text{red}} + \frac{1}{2}m\omega^2 (q^\ddagger - q_{0,\text{red}})^2 = e_{\text{ox}} + \frac{1}{2}m\omega^2 (q^\ddagger - q_{0,\text{ox}})^2 \quad (2.25)$$

From this  $q^\ddagger$  is obtained as

$$q^\ddagger = \frac{1}{2}(q_{0,\text{ox}} + q_{0,\text{red}}) + \frac{e_{\text{ox}} - e_{\text{red}}}{m\omega^2(q_{0,\text{ox}} - q_{0,\text{red}})} \quad (2.26)$$

Then the activation energy  $\Delta g^*$  for the oxidation reaction is obtained as follows:

$$\Delta g^* = U^\ddagger - e_{\text{red}} = \frac{(\lambda + \varepsilon - \varepsilon_F - e\eta)^2}{4\lambda} \quad (2.27a)$$

where  $\varepsilon - \varepsilon_F - e\eta = e_{\text{ox}} - e_{\text{red}}$  and

$$\lambda \equiv \frac{1}{2}m\omega^2 (q_{0,\text{ox}} - q_{0,\text{red}})^2 \quad (2.27b)$$

Here  $\varepsilon$  is the energy states in the electrode metal and  $\eta$  is the overpotential of the electrode.

Substitution of (2.23) for  $N(\varepsilon)$  in (2.21) and combination of (2.27) gives the formula of the current-overpotential relations:

$$\begin{aligned} j = & A[R] \int \rho(\varepsilon) \{1 - f(\varepsilon)\} \exp \left\{ -\frac{(\lambda + \varepsilon - \varepsilon_F - e\eta)^2}{4\lambda kT} \right\} d\varepsilon \\ & - A[O] \int \rho(\varepsilon) f(\varepsilon) \exp \left\{ -\frac{(\lambda - \varepsilon + \varepsilon_F + e\eta)^2}{4\lambda kT} \right\} d\varepsilon \end{aligned} \quad (2.28)$$

After simplifying the equation by replacing the Fermi–Dirac distribution with step function and taking the average of  $\rho(\varepsilon)$ , as  $\rho^*$ , one gets

$$j = 2A\rho^* \sqrt{\lambda kT} \left\{ [R] \operatorname{erfc} \left( \frac{\lambda - e\eta}{2\sqrt{\lambda kT}} \right) - [O] \operatorname{erfc} \left( \frac{\lambda + e\eta}{2\sqrt{\lambda kT}} \right) \right\} \quad (2.29)$$

which shows the limiting currents at high overpotentials. If (2.27) is simplified by taking the energy at the Fermi level  $\varepsilon = \varepsilon_F$ , it is obtained

$$\begin{aligned} j = & \frac{1}{2} A[R] \rho(\varepsilon_F) \exp \left\{ -\frac{(\lambda - e\eta)^2}{4\lambda kT} \right\} - \frac{1}{2} A[O] \rho(\varepsilon_F) \exp \left\{ -\frac{(\lambda + e\eta)^2}{4\lambda kT} \right\} \\ = & k_0[R] \exp \left\{ \frac{\alpha_+(-\lambda + e\eta)}{kT} \right\} - k_0[O] \exp \left\{ -\frac{\alpha_-(\lambda + e\eta)}{kT} \right\} \end{aligned} \quad (2.30a)$$

$$\alpha_+ = \frac{kT}{e} \frac{\partial \ln i_+}{\partial \eta} = \frac{1}{2} - \frac{e\eta}{2\lambda} \quad (2.30b)$$

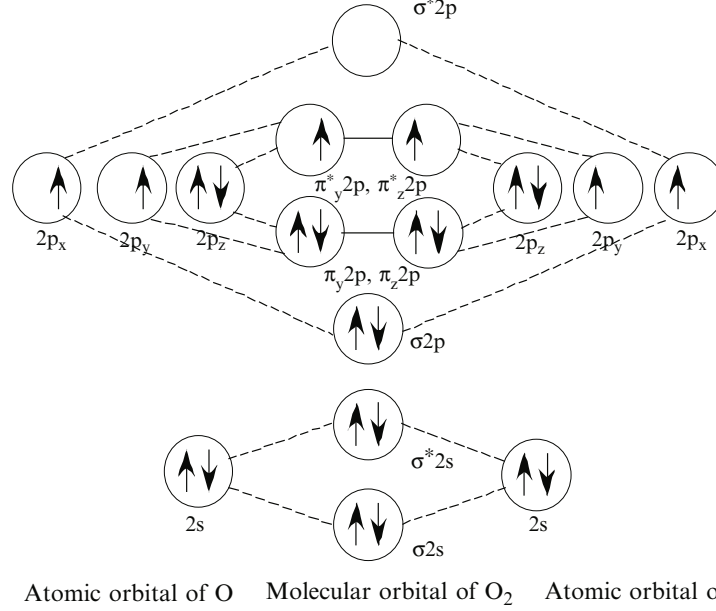
$$\alpha_- = \frac{kT}{e} \frac{\partial \ln i_-}{\partial \eta} = \frac{1}{2} + \frac{e\eta}{2\lambda} \quad (2.30c)$$

which takes the same form as in (2.19) with  $\alpha_+ + \alpha_- = 1$  [25].

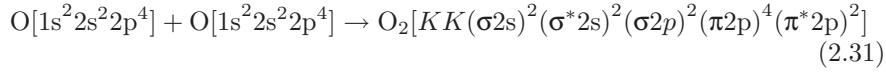
When solvent molecules surround the reacting species, their motion greatly affects the progress of reactions along the reaction coordinate. Increasing the interaction of solvent molecules with the reacting species, the electrode process changes from the outer sphere to inner sphere reactions. The kinetics changes from simple electron transfer to adiabatic processes involving bond-breaking at the electrode. N. S. Hush gives comprehensive overview of this process and presents modification of vibrational contribution in the reorganization energy  $\lambda$  [37].

### 2.4.3 Oxygen Reduction Reaction at Metal Macrocycles

The oxygen atom has the electronic structure of  $(1s)^2(2s)^2(2p)^4$ . Upon forming  $O_2$  molecule the overlap of 2p atomic orbitals gives rise to the molecular orbital (MO) consisting of a  $\sigma_g$  bond and two  $\pi$  bonds, i.e. [38].



**Fig. 2.12.** Molecular orbital of O<sub>2</sub> in the ground state ([38], copyright Clarendon Press)

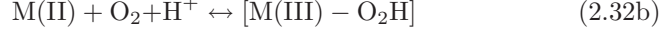


Here  $KK$  denotes filled  $K$  shell of O<sub>2</sub> molecule [ $KK = (\sigma 1s)^2(\sigma^* 1s)^2$ ] and  $*$  denotes antibonding molecular orbital. Filling electrons from the lower level of MO, two unpaired electrons locate in a doubly degenerated  $\pi^*$  antibonding molecular orbital ( $\pi_y^* 2p$  and  $\pi_z^* 2p$ ), forming a triplet ground state (Fig. 2.12). The excess of bonding over nonbonding electrons is four, as seen in the electronic configuration (2.31). The bond order is two with four bonding orbitals and two antibonding orbitals. This explains the high stability of O<sub>2</sub> molecules. When O<sub>2</sub> is reduced on the catalyst surface, the electrons added occupy antibonding orbitals  $\pi^*$  decreasing the bond order and increasing the O–O bond distance [39]. Thus filling in the  $\pi^*$  orbital by increasing the back donation from the d-band metal interacting with O<sub>2</sub> or by shifting the electrode potential to negative directions increases the chance of oxygen reduction reaction.

Macrocycles such as porphyrins and phthalocyanines are biomimetic materials located in the center of heme or cytochrome C, enabling oxygen transport or charge transfer during respiratory reactions [29]. Their ability to adsorb O<sub>2</sub> on the metal center is an important function together with charge transfer through  $N$  ligands in the pyrrole structure.

Oxygen reduction reaction (ORR) on macrocycles is thought to occur via outer-sphere reaction mechanism. As for the reaction mechanism, van Veen

et al. proposed the following schemes [40]:



The number of active sites is potential dependent, and the Nernst equation for the step (2.32a) gives

$$E = E_0 + \frac{RT}{F} \ln \frac{\text{M(III)}}{\text{M(II)}} \quad (2.33)$$

whereas (2.32b) gives, together with (2.33),

$$[\text{M(III)} - \text{O}_2\text{H}] = K_0[\text{O}_2][\text{H}^+][\text{M(III)}] \exp \left\{ -\frac{F(E - E_0)}{RT} \right\} \quad (2.34)$$

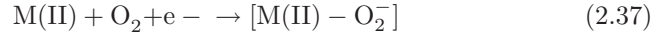
Using (2.19) for the step (2.32c) where only the reduction reaction is taken into account,

$$v = k_0 K_0 [\text{O}_2][\text{H}^+][\text{M(III)}] \exp \left\{ -\frac{(2 - \alpha)F(E - E_0)}{RT} \right\} \quad (2.35)$$

Assuming  $\alpha = 0.5$ , the Tafel slope (slope of the curve of  $E$  vs.  $\log v$ ) as obtained experimentally for iron phthalocyanines,  $-2RT/3F$  ( $-40$  mV at  $25^\circ\text{C}$ ), is explained [40]. If  $\text{M(II)}$  forms in consumption of  $\text{M(III)}$ , i.e.,  $[\text{M(II)}] + [\text{M(III)}] = \text{constant}$ , then another equation results in [cf. (2.18a)]:

$$v = k_0 [\text{O}_2] \frac{\exp \left\{ -\frac{(2 - \alpha)F(E - E_0)}{RT} \right\}}{1 + \exp \left\{ -\frac{F(E - E_0)}{RT} \right\}} \quad (2.36)$$

At large overpotentials, the number of  $\text{M(II)}$  sites becomes potential-independent, and the first one electron-transfer step becomes rate-controlling.



In this case the reaction rate is

$$v = k_0 [\text{O}_2] \exp \left\{ -\frac{(1 - \alpha)F(E - E_0)}{RT} \right\} \quad (2.38)$$

with the Tafel slope of  $-2RT/F$  ( $-120$  mV at  $25^\circ\text{C}$ ). This is the case where ORR occurs at potential much more negative than the  $\text{M(III)}/\text{M(II)}$  couple, and  $\text{H}_2\text{O}_2$  is the main product of the reaction. Zagal et al. discussed the

ORR mechanism on metallophthalocyanines, and suggested that the redox potential,  $pK_a$  of the couples

$$pK_a = \log \left( \frac{[M(III)OH^-][H^+]}{[M(III)][H_2O]} \right) \quad (2.39)$$

and pH of the electrolytes determine the Tafel slopes [41]. In acid media, they assumed that the reaction (2.32b) is rate-determining at low polarization resulting in the Tafel slope of  $-RT/F$  ( $-60$  mV at  $25^\circ\text{C}$ ), while the reaction (2.32a) is rate-determining at high polarization with the Tafel slope of  $-2RT/F$  ( $-120$  mV at  $25^\circ\text{C}$ ). Table 2.3 presents some reported results of Tafel slopes measured for  $O_2$  reduction at transition metal macrocycles.

**Table 2.3.** Reported Tafel slopes in ORR on macrocycles

Macrocycles	Condition	Tafel slope/mV decade <sup>-1</sup>	Major product	Ref.
CoTAA	0.5 M H <sub>2</sub> SO <sub>4</sub> , 25°C	-60	H <sub>2</sub> O	[42]
Fe polyphtalocyanine	6 M KOH, 25°C	-85	—	[43]
CoTSP	0.05 M H <sub>2</sub> SO <sub>4</sub> , 20°C	-135	H <sub>2</sub> O <sub>2</sub>	[44]
	0.1 M NaOH, 20°C	-120	H <sub>2</sub> O <sub>2</sub>	
CoTSP	0.05 M H <sub>2</sub> SO <sub>4</sub> , 25°C	-155	H <sub>2</sub> O <sub>2</sub>	
	M NaOH, 25°C	-120	H <sub>2</sub> O <sub>2</sub>	[41]
FeTSP	0.05 M H <sub>2</sub> SO <sub>4</sub> , 25°C	-65	H <sub>2</sub> O <sub>2</sub>	
	0.1 M NaOH, 25°C	-30 to -35	H <sub>2</sub> O <sub>2</sub>	
CoTPP	0.5 M HClO <sub>4</sub> + 0.5	-120	H <sub>2</sub> O <sub>2</sub>	[45]
CoTPP + 4Ru(NH <sub>3</sub> ) <sub>5</sub> <sup>2+</sup>	M NH <sub>4</sub> PF <sub>6</sub>	-90	H <sub>2</sub> O	
Pyrolyzed CoTMPP	0.3 M HClO <sub>4</sub> , RT	-52 to -61	H <sub>2</sub> O	
Pyrolyzed CoPc		-70 to -149	H <sub>2</sub> O	[46]
Pyrolyzed CoCy		-110 to -141	H <sub>2</sub> O <sub>2</sub>	
Poly(CoTAPP)	0.5 M H <sub>2</sub> SO <sub>4</sub> , 20°C	-58 (low $\eta$ )	H <sub>2</sub> O <sub>2</sub>	[47]
Poly(CoTAPc)		-116 (high $\eta$ )	H <sub>2</sub> O <sub>2</sub>	
Pyrolyzed	0.5 M H <sub>2</sub> SO <sub>4</sub> , 20°C	-60 (low $\eta$ )	H <sub>2</sub> O <sub>2</sub>	
CoTMeOPP		-120 (high $\eta$ )		[48]
	1 M KOH, 20°C	-40 (low $\eta$ )	H <sub>2</sub> O	
		-120 (high $\eta$ )		
FePc	0.5 M H <sub>2</sub> SO <sub>4</sub> , 20°C	-65	H <sub>2</sub> O	
		-121	H <sub>2</sub> O	[49]
Heat-treated FePc		-63		

CoTAA: cobalt dibenzotetraazaannulene, Co(Fe)TSP: cobalt (iron) tetrasulfonate phthalocyanine, CoTPP: cobalt tetrapyridylporphyrin, CoTMPP: cobalt tetramethoxyphenylporphyrin, CoPc: cobalt phthalocyanine, CoCy: cobalt cyclam, CoTAPP: cobalt tetra(*o*-aminophenyl)porphyrin, CoTAPc: cobalt 4, 4', 4'', 4'''-tetraaminophthalocyanine, CoTMeOPP: cobalt 5,10,15,20-tetra(methoxyphenyl)porphyrin, FePc: iron phthalocyanine

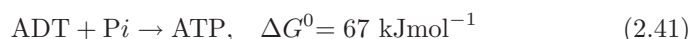
## 2.5 Proton Transport in Polymer Electrolytes

### 2.5.1 Proton Transfer Reactions

For photosynthesis and adenosine-triphosphate (ATP) production at plant cells, P. Mitchell proposed a mechanism in which the  $H^+$  motive force across the chloroplast membrane is utilized as the energy required for the oxidative phosphorylation of adenosine-diphosphate (ADP) [50]. During the charge separation by the light energy, the proticity (proton-motive force)  $\Delta P$  produces electric potential  $\Delta\psi$  and  $H^+$  driving force  $\Delta pH$  that is accumulated across the membrane (active transport of  $H^+$ ) [51]:

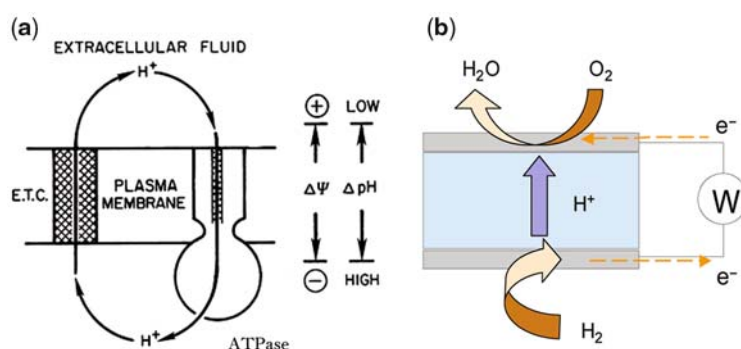
$$\Delta P = \Delta\psi - \frac{2.3RT}{F}\Delta pH \quad (2.40)$$

i.e., energy liberated during the electron transport by redox reactions is stored as  $\Delta pH$ . ATP is synthesized as a dark reaction, at the consumption of the electrochemical potential difference of  $H^+$  across the membrane (Fig. 2.13a).



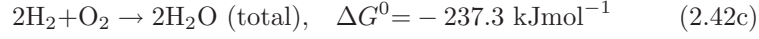
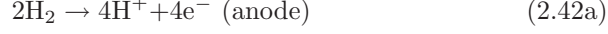
where  $Pi$  represents inorganic orthophosphate. The coupling of electron and proton transports plays an important role in ATP synthesis [29, 52]. F rland et al. point out that the energy conversion efficiency from redox reaction to ATP synthesis is as high as 0.96, and the process takes place in close to equilibrium conditions [53].

This is in close resemblance to fuel cell systems, where the chemical reactions are converted into the electric potential,



**Fig. 2.13.** (a) Chemiosmotic proton translocation model for ATP synthesis in which electron transport chain and proton conduction pathway are coupled ([51], copyright Plenum Press). (b) Energy conversion in fuel cells in which chemical energy of fuel oxidation is converted to electricity by a coupled transport of electron in the outer circuit and proton in the polymer electrolyte membrane



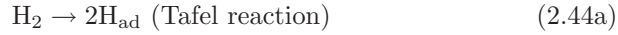


$$E_{\text{rev}}^0 = -\Delta G^0 / 4F = 1.23 \text{ V} \quad (2.43)$$

which drives the  $\text{H}^+$  transport across the membrane (Fig. 2.13b). In the case of the chloroplast membrane,  $\text{H}^+$  is transported through the proton channel formed across the membrane, and this is coupled to the ATP production. In fuel cell membranes (polymer electrolyte membrane or proton exchange membrane, PEM),  $\text{H}^+$  is driven by the potential difference across the membrane that separates the  $\text{H}_2$  and the  $\text{O}_2$  gas electrodes. Since  $\text{H}^+$  mediates the reactions at the anode and the cathode as in (2.42a) and (2.42b), its conduction sometimes limits the overall fuel cell current.

Although the transmembrane potential in normal biological systems is of the order far less than 100 mV, mitochondria or chloroplast membranes show 200 mV for  $\Delta P$ . This large potential would not be a result of Nernstian diffusion potential but significantly by a surface charge potential [51]. According to the chemiosmotic hypothesis by P. Mitchell, the electron transport proteins and the proton ATPase complex, which are incorporated in a bilayer structure of a cell membrane, are coupled so that electrogenic pumping of  $\text{H}^+$  creates a high  $\Delta P$  as in (2.40). This high  $\Delta P$  drives the synthesis of ATP as  $\text{H}^+$  flows down along a proton conduction pathway in the ATPase [51]. Whether or not  $\text{H}^+$  migrates faster in the membrane than in aqueous solution, and how so in sub-molecular level, is a central question not answered yet.

Proton transfer at the catalyst surface is an important topic in relation to energy conversion systems such as fuel cell catalysts, photoexcited water splitting, and electrochemical solar cells.  $\text{H}^+$  ion discharge at the metal electrodes occurs in two steps:



or



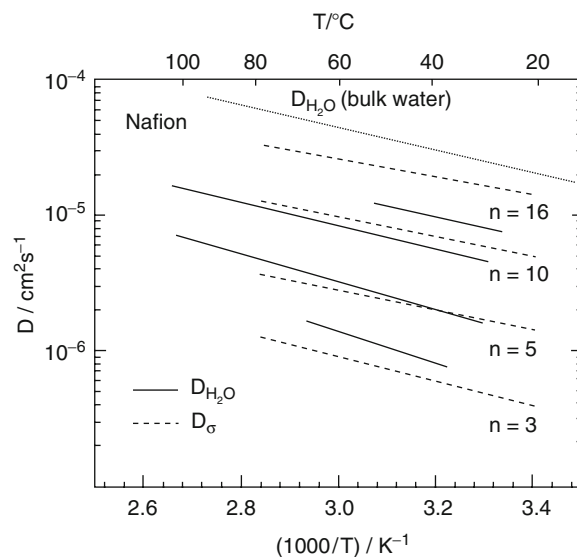
followed by



The subject was reviewed for hydrogen evolution reactions [54,55] and for hydrogen oxidation reactions [56], also briefly in Chap. 1.

### 2.5.2 Proton Transport in Polymer Electrolytes

A number of investigations are reported about the structure and  $\text{H}^+$  conduction mechanism in PEM, made of perfluorosulfonated ionomers [57,58]. Since this is a phase-separated membrane with inverse micelle microstructures,  $\text{H}^+$  is preferentially conducted through the water-containing ionic channels of about 4 nm domains connected by 1 nm channels [59]. Figure 2.14 depicts diffusion



**Fig. 2.14.** Proton conductivity diffusion coefficient (mobility) and water self-diffusion coefficient of Nafion 117 (EW = 1100 g/equiv), as a function of temperature and the degree of hydration ( $n = [\text{H}_2\text{O}]/[-\text{SO}_3\text{H}]$ ) ([57], copyright the American Chemical Society)

coefficients for  $\text{H}^+$  transport and for water molecules in Nafion 117 membranes [57]. At high water content,  $\text{H}^+$  transfers by Grotthuss mechanism (an interchange between  $\text{H}_3\text{O}^+$  and  $\text{H}_2\text{O}$  for  $\text{H}^+$  movement) through the bulk-like water in the ionic channel, and its diffusion is faster than  $\text{H}_2\text{O}$ . With decreasing water content,  $\text{H}^+$  transport is suppressed and becomes of vehicular mechanism. This fact indicates a strong interaction of  $-\text{SO}_3^-$  and  $\text{H}_2\text{O}$ .

The state of water inside of PEM strongly affects  $\text{H}^+$  conduction, indicating a coupled transport of  $\text{H}^+$  and  $\text{H}_2\text{O}$ . This is confirmed by measuring the water drag coefficient  $t_{\text{H}_2\text{O}}$  (number of  $\text{H}_2\text{O}$  carried with  $\text{H}^+$ ) [60]. Table 2.4 summarizes the transport parameters measured in perfluorosulfonated ionomer membranes. The ion-exchange capacity (IEC), i.e., density of sulfonic acid groups has a strong influence on the transport parameters. When the ion-exchange capacity increases,  $\text{H}^+$  conductivity and water content increases. In comparison to this, the ratio of nonfreezing water, which is defined as the water not frozen even when the membrane is cooled down below  $-20^\circ\text{C}$ , and is assumed as the water strongly interacting with  $\text{H}^+$  and  $-\text{SO}_3^-$  sites, does not increase much. The result implies that channel volume and unbound water are critical factors for  $\text{H}^+$  conduction, together with  $t_{\text{H}_2\text{O}}$  [60, 61]. Design of a high  $\text{H}^+$  conducting PEM is to be accomplished by tailoring main chain and side chain units and by partial cross-linking, thus controlling the ionic channel structures [60]. However, in order to achieve higher performance membranes,

**Table 2.4.** Characteristic properties of perfluorinated ionomer membranes in fully hydrated state

Membrane IEC <sup>a</sup> /meq g <sup>-1</sup>	PFSI A 0.91	PFSI B1 0.91	PFSI B2 1.1
Thickness (wet state)/ $\mu\text{m}$	220	205	150
Water content <sup>b</sup> / $n\text{H}_2\text{O}$ ( $n\text{SO}_3^-$ ) <sup>-1</sup>	20.8	19.1	23.6
Nonfreezing water <sup>c</sup> / $n\text{H}_2\text{O}$ ( $n\text{SO}_3^-$ ) <sup>-1</sup>	12.5–13.1	11.4–11.9	14.7–15.3
Ratio of nonfreezing water	0.61	0.61	0.63
H <sup>+</sup> conductivity <sup>d</sup> $\kappa/\text{S cm}^{-1}$	0.15	0.14	0.19
Activation energy of H <sup>+</sup> conduc- tion $E_a(\text{H}^+)/\text{kJ mol}^{-1}$	8.7	8.9	7.6
H <sub>2</sub> O diffusion coefficient <sup>e</sup> $D_{\text{H}_2\text{O}}/\text{m}^2 \text{s}^{-1}$	$7.1 \times 10^{-10}$	$5.7 \times 10^{-10}$	$8.6 \times 10^{-10}$
Activation energy of H <sub>2</sub> O trans- port $E_a(\text{H}_2\text{O})/\text{kJ mol}^{-1}$	20.0	19.6	18.8
Water transference coefficient <sup>f</sup> $t_{\text{H}_2\text{O}}$	3.11	2.96	3.21

<sup>a</sup>Mole of  $\text{SO}_3^-$  per gram of dry membrane<sup>b</sup>Number of moles of  $\text{H}_2\text{O}$  per mole of  $\text{SO}_3^-$ <sup>c</sup>Number of moles of  $\text{H}_2\text{O}$  per mole of  $\text{SO}_3^-$  that does not freeze down to  $-20^\circ\text{C}$  (determined from DSC curves [61])<sup>d</sup>Determined by AC impedance method at  $25^\circ\text{C}$  [60]<sup>e</sup>Determined by PG-NMR method at  $30^\circ\text{C}$  [61]<sup>f</sup>Number of moles of  $\text{H}_2\text{O}$  dragged per mole of  $\text{H}^+$  (determined by streaming potential method at  $25^\circ\text{C}$  [60])

for example high temperature  $\text{H}^+$  conducting polymer electrolytes where no  $\text{H}_2\text{O}$  may participate, some biomimetic concepts should be applied to give a solution. A model would be the  $\text{H}^+$ -conducting pathway in the cell membrane, in which a special structure for  $\text{H}^+$  hopping conduction should play a role.

## 2.6 Summary

Charge transport (CT) by or between redox molecules in a heterogeneous phase have been described. Depending on the materials and systems, various methodologies and theories have been adopted to analyze CT processes. CT is classified mainly into two categories, one is charge propagation in a matrix that is of importance in electronic and energy conversion devices, and the other is a single-step charge transfer between molecules important in biological and its mimetic systems as well as in fundamental redox chemistries.

The former charge propagation is a successive multistep charge transport in a matrix essential for the system to function as a practical device. Such charge propagation is often investigated by electrochemical methods. A single-step charge (often electron) transfer between two molecules is a key process in biological activities and also in chemical reactions. This electron-transfer event is often studied by a laser flash photolysis or by utilizing other photoexcited state phenomena since the process is often very rapid, but electrochemical measurements are of course a powerful tool for this purpose. A successive electron transfer between different redox molecules resulting in multi-gearred cycles plays a key role in biological activities. Well-designed and sophisticated multi-gearred charge transfer cycles utilizing functional molecules would definitely promise us innovative energy-conversion devices capable of resolving the big issue of global warming threatening our civilization now.

Controlling the charge transfer in macrocycles and other metal complexes is the major task in order to improve the rate of energy conversion in fuel cell reactions. This should be achieved by designing ligands that mediate an efficient electron transfer between metal centers and reactants that show intrinsically different energy levels. The reaction mechanism and rate-determining step should change depending on the ligand structure, which can be evaluated by redox potentials of the complexes or Tafel slopes in the polarization curves. Proton transport is also an important topic in relation to biological membranes and fuel cell electrolytes. Elucidation of detailed mechanism and its application in membrane designing would give broad range of possibilities in accomplishing materials based on a biomimetic concept.

## References

1. C. Nicolini, *Biophysics of Electron Transfer and Molecular Bioelectronics* (Plenum, New York, 1998)
2. M. Graetzel, K. Kalyanasundaram, *Curr. Sci.* **66**, 706 (1994)
3. G.J. Meyer, *Molecular Level Artificial Photosynthetic Materials Progress in Inorganic Chemistry* (Wiley-Interscience, New York, 1997)
4. M. Yagi, M. Kaneko, *Adv. Polym. Sci.* **199**, 143 (2006)
5. M. Yagi, M. Kaneko, *Chem. Rev.* **101**, 21 (2001)
6. T. Abe, M. Kaneko, *Prog. Polym. Sci.* **28**, 1441 (2003)
7. M. Kaneko, in *Metal Complexes and Metals in Macromolecules* chap. 14, ed. by D. Woehrle, A.D. Pomogailo (Wiley-VCH, Weinheim, 2006)
8. H.J. Dahms, *J. Phys. Chem.* **72**, 362 (1968)
9. I. Ruff, J. Friedlich, *J. Phys. Chem.* **75**, 3297 (1971)
10. C.P. Andrieux, J.M. Saveant, *J. Electroanal. Chem.* **11**, 377 (1980)
11. D.N. Blauch, J.M. Saveant, *J. Am. Chem. Soc.* **114**, 3323 (1992)
12. J. Zhang, F. Zhao, M. Kaneko, *J. Porphyrins Phthalocyanines* **3**, 1 (1999)
13. F. Zhao, J. Zhang, T. Abe, M. Kaneko, *J. Porphyrins Phthalocyanines* **3**, 238 (1999)
14. M.J. Therien, M. Selman, H.B. Gray, *J. Am. Chem. Soc.* **112**, 2420 (1990)

15. D.N. Beratan, J.N. Onuchic, J.N. Betts, B.E. Bowler, H.B. Gray, *J. Am. Chem. Soc.* **112**, 7915 (1990)
16. R.A. Marcus, *J. Chem. Phys.* **24**, 966 (1955); **43**, 679 (1956)
17. O. Stern, M. Volmer, *Phys. Z.* **20**, 183 (1919)
18. N.J. Turro, *Modern Molecular Photochemistry* (Benjamin/Cummings, Menlo Park, 1978)
19. J. Perrin, *Comp. Rend. Acad. Sci. Paris* **184**, 1097 (1924); **178**, 1978 (1927)
20. K. Nagai, N. Takamiya, M. Kaneko, *Macromol. Chem. Phys.* **197**, 2983 (1996)
21. K. Nagai, N. Tsukamoto, N. Takamiya, M. Kaneko, *J. Phys. Chem.* **99**, 6648 (1995)
22. T. Abe, T. Ohshima, K. Nagai, S. Ishikawa, M. Kaneko, *React. Funct. Polym.* **37**, 133 (1998)
23. E. Leiva, S. Sánchez, in *Handbook of Fuel Cells – Fundamentals, Technology and Applications* vol. 2, chap. 12, ed. by W. Vielstich, H.A. Gasteiger, A. Lamm (Wiley, Chichester, 2003)
24. R.A. Marcus, *J. Electroanal. Chem.* **483**, 2 (2000)
25. J. Koryta, J. Dvořák, L. Kavan, *Principles of Electrochemistry* chap. 5 (Wiley, Chichester, 1987)
26. S. Larsson, *J. Chem. Soc. Faraday Trans.* **2**, 1375 (1983)
27. P.F. Barbara, T.J. Meyer, M.A. Ratner, *J. Phys. Chem.* **100**, 13148 (1996)
28. S. Roth, in *Hopping Transport in Solids*, chap. 11, ed. by M. Pollak, B. Shklovskii (Elsevier, Amsterdam, 1991)
29. L. Stryer, *Biochemistry* (W. H. Freeman, San Francisco, 1975)
30. A.J. Bard, L.R. Faulkner, *Electrochemical Methods, Fundamentals and Applications*, chap. 3 (Wiley, New York, 1980)
31. R.W. Gurney, *Proc. Roy. Soc.* **A134**, 137 (1931)
32. J.E.B. Randles, *Trans. Faraday Soc.* **48**, 828 (1952)
33. H. Gerischer, *Z. Phys. Chem. NF* **26**, 223, 325 (1960)
34. V.G. Levich, in *Physical Chemistry: An Advanced Treatise*, vol. IXB, chap. 12, ed. by H. Eyring, D. Henderson, W. Jost (Academic Press, New York, 1970)
35. J. Goodisman, *Electrochemistry: Theoretical Foundations* (Wiley, New York, 1987)
36. A.J. Appleby, in *Modern Aspects of Electrochemistry*, vol. 9, chap. 5 ed. by B.E. Conway, M. Bockris JO' (Plenum, New York, 1974)
37. N.S. Hush, *J. Electroanal. Chem.* **460**, 5 (1999)
38. C.A. Coulson, *Valence*, chap. 4 (Clarendon Press, Oxford, 1961)
39. J.H. Zagal, *Coord. Chem. Rev.* **119**, 89 (1992)
40. J.A.R. van Veen, J.F. van Baar, C.J. Kroese, J.G.F. Coolegem, N. de Wit, H.A. Colijn, *Ber. Bunsenges. Phys. Chem.* **85**, 693 (1981)
41. J. Zagal, P. Bindra, E. Yeager, *J. Electrochem. Soc.* **127**, 1506 (1980)
42. F. Beck, *J. Appl. Electrochem.* **7**, 239 (1977)
43. A.J. Appleby, M. Savy, *Electrochim. Acta* **22**, 1315 (1977)
44. J. Zagal, R.K. Sen, E. Yeager, *J. Electroanal. Chem.* **83**, 207 (1977)
45. C. Shi, F.C. Anson, *Electrochim. Acta* **39**, 1613 (1994)
46. E. Claude, T. Addou, J.M. Latour, P. Aldebert, *J. Appl. Electrochem.* **28**, 57 (1997)
47. O.E. Mouahid, C. Coutanceau, E.M. Belgsir, P. Crouigneau, J.M. Léger, C. Lamy, *J. Electroanal. Chem.* **426**, 117 (1997)
48. M.R. Tarasevich, K.A. Radyushkina, G.V. Zhutaeva, *Russian J. Electrochem.* **40**, 1174 (2004)

49. S. Baranton, C. Coutanceau, E. Garnier, J.M. Léger, J. Electroanal. Chem. **590**, 100 (2006)
50. P. Mitchell, Nature **191**, 144 (1961)
51. R. Pethig, in *Modern Bioelectrochemistry*, chap.7, ed. by F. Gutmann, H. Keyzer (Plenum Press, New York, 1986)
52. S. Ohki, in *Comprehensive Treatise of Electrochemistry*, vol. 10, chap. 1, ed. by S. Srinivasan, YuA. Chizmadzhev, M. Bockris JO', B.E. Conway, E. Yeager (Plenum Press, New York, 1985)
53. K.S. Førlund, T. Førlund, S. Kielstrup-Ratkje, *Irreversible Thermodynamics*, chap. 10 (Wiley, Chichester, 1988)
54. H. Kita, T. Kurisu, J. Res. Inst. Catalysis, Hokkaido Univ. **21**, 200 (1973)
55. J. Horiuti, in *Physical Chemistry An Advanced Treatise*, vol. IXB, chap. 6, ed. by H. Eyring, D. Henderson, W. Jost (Academic Press, New York, 1970)
56. M.W. Breiter, in *Handbook of Fuel Cells – Fundamentals, Technology and Applications*, vol. 2, chap. 25, ed by W. Vielstich, H.A. Gasteiger, A. Lamm (Wiley, Chichester, 2003)
57. K.D. Kreuer, S.J. Paddison, E. Spohr, M. Schuster, Chem. Rev. **104**, 4637 (2004)
58. K.A. Mauritz, R.B. Moore, Chem. Rev. **104**, 4535 (2004)
59. \*T.D. Gierke, W.Y. Hsu, (1982) In: Eisenberg A, Yeager HL (eds) Perfluorinated Ionomer Membranes. ACS Symposium Series 180, Am. Chem. Soc., Washington DC, chap. 13
60. T. Okada, M. Saito, K. Hayamizu, in *Electroanalytical Chemistry Research Developments*, ed by P.N. Jiang chap. 2 (Nova Science, New York, 2007)
61. M. Saito, K. Hayamizu, T. Okada, J. Phys. Chem. B **109**, 3112 (2005)